

Influence on the Temperature Estimation by the Planetary Boundary Layer Scheme with Different Minimum Eddy Diffusivity in WRF v3.9.1.1: Supplement

Hongyi Ding¹, Le Cao^{1,*}, Haimei Jiang¹, Wenxing Jia^{1,3}, Yong Chen², and Junling An²

¹Key Laboratory for Aerosol-Cloud-Precipitation of China Meteorological Administration, Nanjing University of Information Science and Technology, Nanjing 210044, China

²State Key Laboratory of Atmospheric Boundary Layer Physics and Atmospheric Chemistry, Institute of Atmospheric Physics, Chinese Academy of Sciences, Beijing 100029, China

³Key Laboratory of Atmospheric Chemistry of CMA, Chinese Academy of Meteorological Sciences, Beijing 100081, China

Correspondence: L. Cao
(le.cao@nuist.edu.cn)

S1 Temporal Evolution of PM_{2.5} in Beijing Area in January, 2014

Figure S1 displays the temporal change in the PM_{2.5} concentration in the region of Beijing, China in January, 2014. It can be seen in Fig. S1 that in time periods of Jan. 8-15 and Jan. 20-24, the concentration of PM_{2.5} accumulates, which reflects relatively stagnant weather conditions in this area at these time stages. In contrast, in other time periods, the PM_{2.5} concentration mostly drops, denoting a unsettled weather condition. In addition, on Jan, 16, a precipitation occurs, which screens out the possibility of adopting this day for the present simulation. Thus, in this study, we used the two time periods (Jan. 8-15 and Jan. 20-24, 2014) representing the stagnant weather conditions in this area for the investigation.

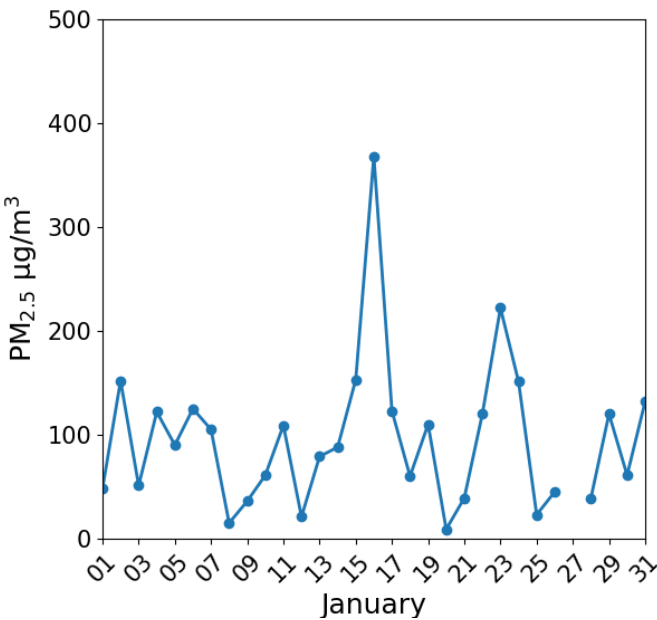


Figure S1. Temporal evolution of the PM_{2.5} concentration over the Beijing area in January, 2014.

S2 Spatial Distributions of the Land-Use Fraction for the Urban Category and the Calculated $PURB$

The spatial distributions of the land-use fraction for the urban category (i.e. $Landusef(Urban)$) and the calculated $PURB$ are shown in Fig. S2. The value of the urban fraction (i.e. $Landusef(Urban)$) resides in a range between 0 and 1 for each grid cell, and $PURB$ is calculated according to Eqs. (6) and (7) given in the manuscript.

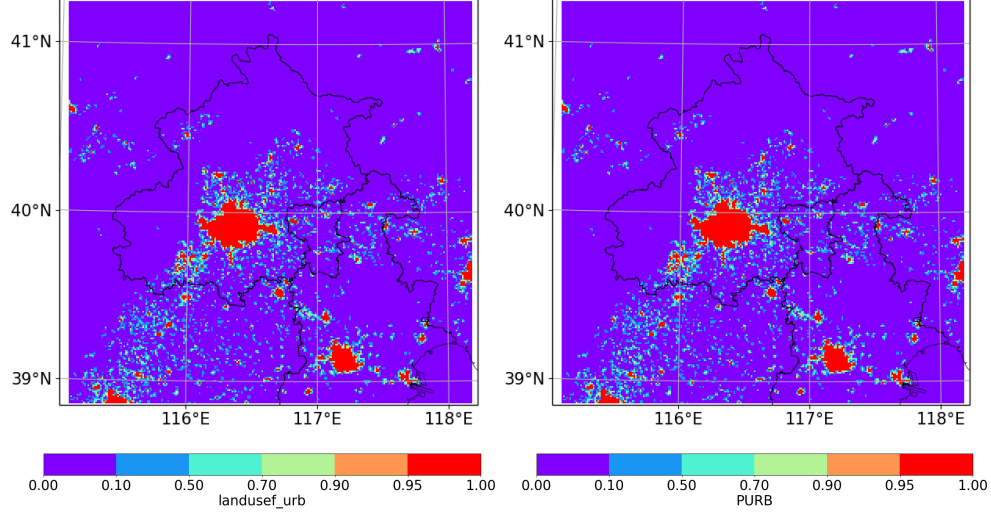


Figure S2. The spatial distributions of the land-use fraction for the urban category (i.e. $Landusef(Urban)$) and the calculated $PURB$ in the innermost computational domain.

S3 Model Evaluations for Simulating the 2-m Temperature and the 10-m Wind Speed

Figure S3 shows the diurnal change in the averaged T2 at five stations (IAP station and four automatic weather stations (AWS)) as well as the observations. It can be seen that at these stations, the highest T2 appears at approximately 15 local standard time (LST), while the lowest T2 appears at around 8 LST. This is also the reason why we focused on these two time points in the present study. Moreover, it was found that at the three rural stations (No. 54406, 54419 and 54501), the simulated 2-m temperature is higher than the observational value in the nighttime, while it is lower than the observation during the daytime when the temperature is high. As a result, the simulated diurnal variation of T2 at the rural stations is weaker than the observations. On the contrary, at two urban stations, the cold bias appears during the whole day.

With respect to the 10-m wind speed, Fig. S4 shows the spatial distribution of the time-averaged 10-m wind speed over the nighttime. It was found that a larger wind speed is estimated in mountain areas than in plain areas, leading to the formation of a stronger wind shear in mountain areas rather than in plain areas.

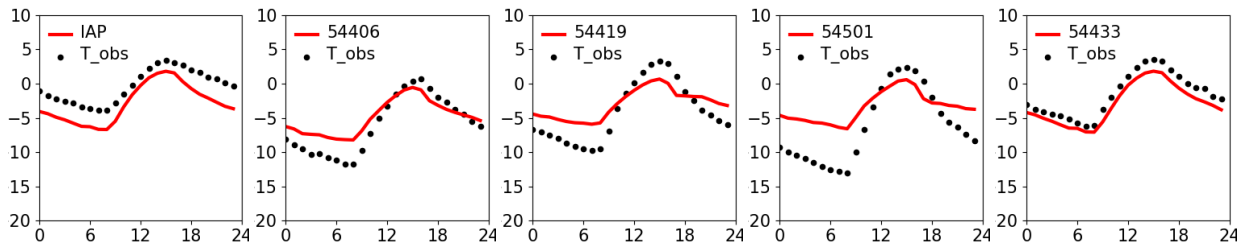


Figure S3. Diurnal change in the time-averaged 2-m temperature (T2) obtained from simulations and observations at five stations.

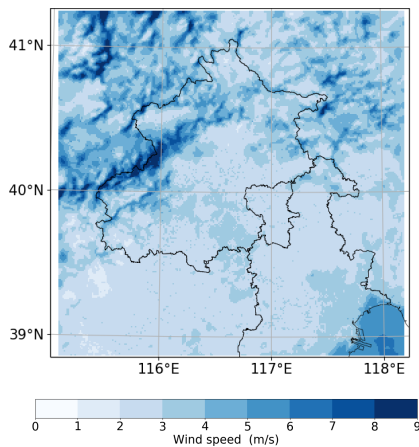


Figure S4. The spatial distribution of the time-averaged 10-m wind speed over the nighttime.

S4 Influence of Changing K_{zmin} on the 10-m Wind Speed (WS) and the 2-m Specific Humidity (Q2)

The values of statistical parameters for simulations of 2-m temperature ($^{\circ}\text{C}$), 10-m wind speed (m s^{-1}) and 2-m specific humidity (i.e. Q2) (g kg^{-1}) are listed in Tab. S1. It can be seen that the changes in the wind speed and the specific humidity caused by the altering of K_{zmin} are significantly smaller than that in the 2-m temperature. Thus, we paid more attention to the influence on the temperature prediction brought by the change in K_{zmin} at present.

Table S1. Values of statistical parameters measuring the model performance in simulating 2-m temperature ($^{\circ}\text{C}$), 10-m wind speed (m s^{-1}) and 2-m specific humidity (g kg^{-1}).

K_{zmin}	T2				W10				Q2			
	RMSE	IOA	R	MB	RMSE	IOA	R	MB	RMSE	IOA	R	MB
0.01	2.79	0.84	0.94	-2.49	3.21	0.26	0.64	2.51	0.21	0.85	0.73	0.02
0.2	2.32	0.88	0.93	-2.00	3.27	0.26	0.62	2.60	0.21	0.84	0.72	0.01
0.5	2.01	0.90	0.92	-1.58	3.31	0.25	0.63	2.70	0.21	0.85	0.73	0.01
0.8	1.88	0.91	0.90	-1.27	3.38	0.25	0.62	2.77	0.20	0.85	0.74	0.01
1.0	1.82	0.91	0.89	-1.08	3.39	0.25	0.62	2.79	0.20	0.86	0.75	0.00

The time series of the 10-m wind speed and the 2-m specific humidity (i.e. Q2) simulated by five scenarios using different constant values of K_{zmin} are shown in Fig. S5. In general, the increase of K_{zmin} exerts a relatively less influence on the changes in the wind speed and the specific humidity, compared with the change in the temperature. It means that the simulation accuracy of the wind speed and the specific humidity is not heavily influenced by the change in K_{zmin} . It was also found in Fig. S5 that the increase of K_{zmin} induces a stronger 10-m wind speed. In contrast, the simulated Q2 was found lower under a higher K_{zmin} . It is because that a larger K_{zmin} causes a stronger mixing. As a result, the momentum is transported downwards from higher altitudes and the moisture is transported upwards from the altitude near the surface. Thus, a larger 10-m wind speed and a lower Q2 were obtained when a higher K_{zmin} is applied in the model.

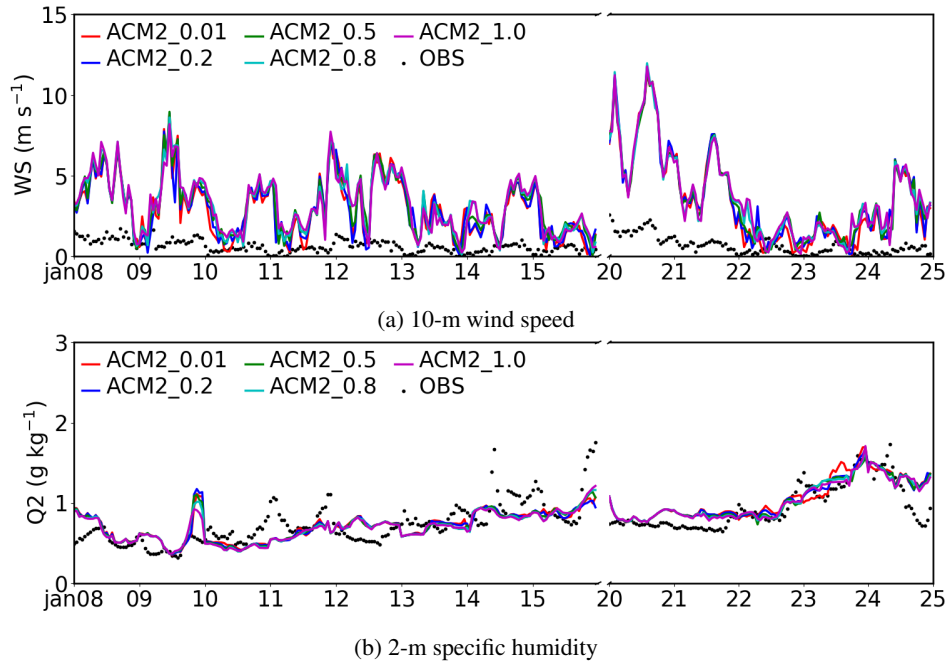


Figure S5. Time series of 10-m wind speed (WS) and 2-m specific humidity (Q2) estimated by five scenarios with different $K_{z\min}$ values.

S5 Diurnal Variation of the Downward Shortwave Radiation at the Ground Surface

The diurnal change in the downward shortwave radiation at the ground surface in scenarios using different K_{zmin} values is shown in Fig. S6. It can be seen that the difference in the downward shortwave radiation during the daytime between these scenarios is negligible. It means that the influences exerted by the shortwave radiation in the daytime under the conditions of
40 various K_{zmin} settings are similar, which screens out the possibility that the shortwave radiation is responsible for the large deviation in the nighttime temperature prediction between these scenarios.

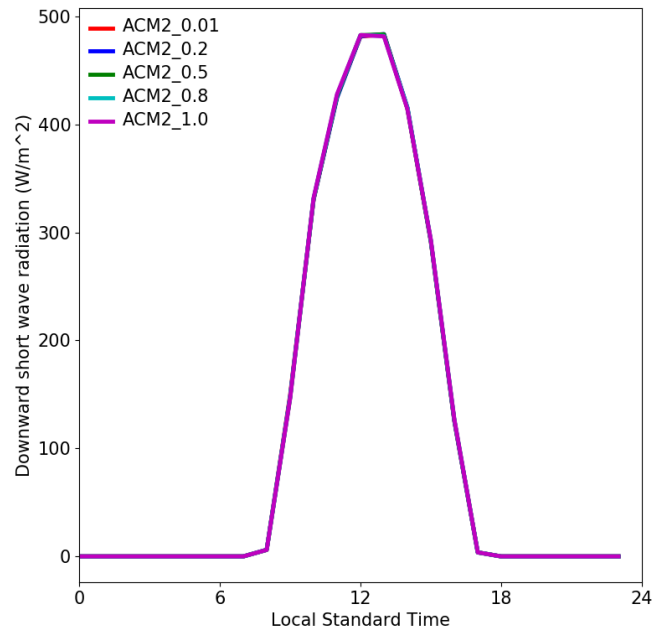


Figure S6. The diurnal change in the downward shortwave radiation reaching the ground surface, simulated by using different K_{zmin} values.

S6 Temperature Tendencies Caused by Net Longwave Radiation

We first output the hourly-averaged temperature tendencies caused by the change in the net longwave radiation at all model levels under the conditions of different K_{zmin} values, and we found the difference in the temperature tendencies more pronounced near the surface, which means that the change caused by the net longwave radiation under different K_{zmin} conditions is more obvious at the first layer of the model.

We then plotted the diurnal change of temperature tendencies due to the net longwave radiation at the first model layer, given by ACM2_0.01 and ACM2_1.0 (see Fig. S7), to assess the contribution of the net longwave radiation to the difference in the near-surface temperature between scenarios using different K_{zmin} values. In Fig. S7, negative temperature tendencies were found in both of these two scenarios during the nighttime. It means that at the first model layer, the net longwave radiation leads to a loss of the net energy at night. Moreover, Fig. S7 shows that the temperature tendency of ACM2_1.0 is lower than that of ACM2_0.01 during the nighttime. It means that the decrease of temperature caused by the net longwave radiation in ACM2_1.0 is more rapid than that in ACM2_0.01. As a result, the influence of the net longwave radiation is to reduce the temperature difference between these two scenarios, especially during the nighttime, as ACM2_1.0 estimates a higher first-level temperature at night than ACM2_0.01. Thus, the net longwave radiation is not the factor causing the enlarged temperature difference between the nighttime simulations of ACM2_1.0 and ACM2_0.01.

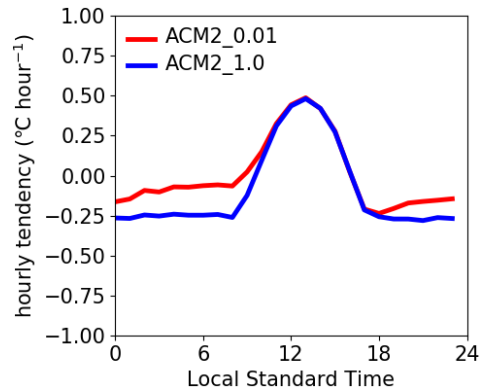


Figure S7. Diurnal variation of the hourly-averaged temperature tendencies caused by the net longwave radiation at the first model layer, given by ACM2_0.01 and ACM2_1.0.

S7 Spatial Distribution of the Friction Velocity

The spatial distribution of the time-averaged friction velocity (u_*) over the nighttime belonging to the simulation scenario of ACM2_0.01 is shown in Fig. S8. From Fig. S8, we can see that during the nighttime, the friction velocity in mountain areas is larger than that in plain areas. It denotes that a larger wind shear is generated in mountain areas rather than in plain areas, resulting in a larger turbulent diffusivity K_z in mountain areas. As a result, the change in $K_{z\min}$ exerts a relatively less impact in mountain areas than in plain areas.

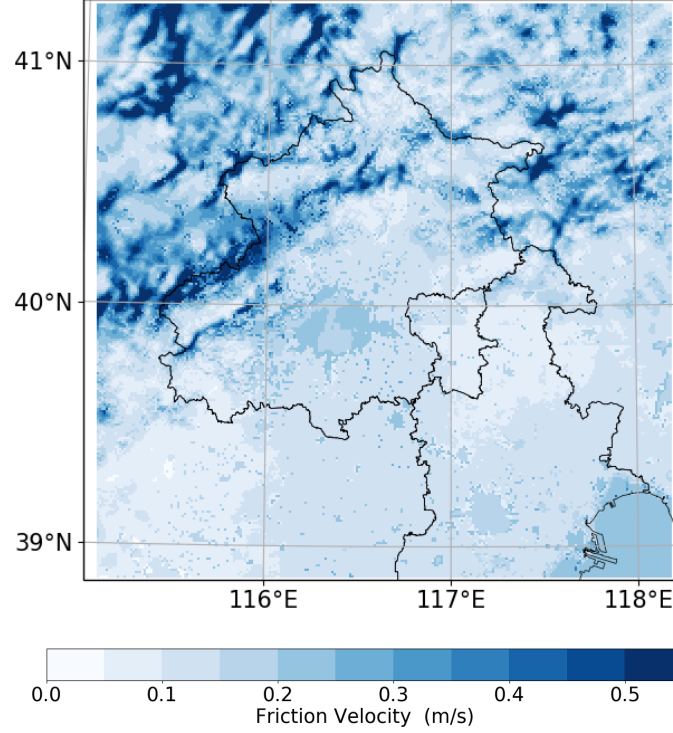


Figure S8. The spatial distribution of the mean friction velocity during the nighttime, when the value of $K_{z\min}$ is set to 0.01.

S8 Spatial Distribution of the Vertical Turbulent Diffusivity (K_z)

The spatial distribution of the time-averaged vertical turbulent diffusivity (K_z) over the nighttime belonging to the simulation scenario of ACM2_0.01 is shown in Fig. S9. From Fig. S9, we can see that in the nighttime, the vertical turbulent diffusivity in mountain areas is mostly stronger than that in plain areas, so that the increase of $K_{z\min}$ would exert a less influence on the change of the turbulent diffusivity as well as the 2-m temperature (T2) in mountain areas than in plain areas.

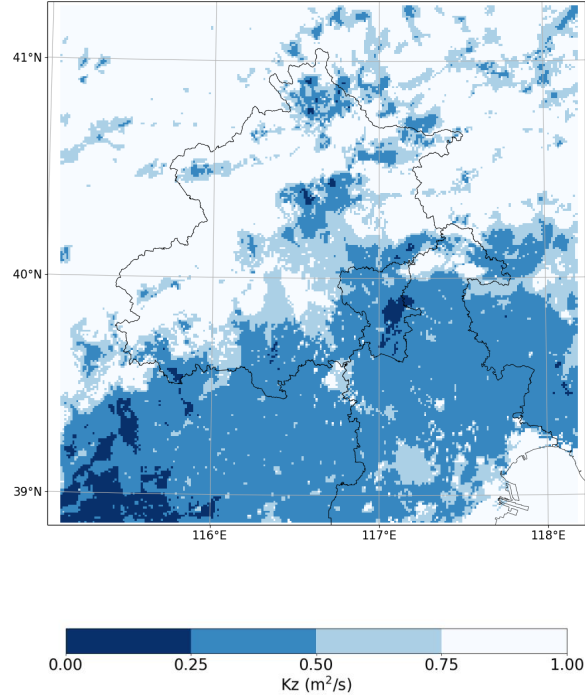


Figure S9. The spatial distribution of the mean vertical turbulent diffusivity (K_z) during the nighttime, when the value of $K_{z\min}$ is set to 0.01.